Supporting Information

Decreasing Coordinated N Atoms in Single-Atom Cu Catalyst to Achieve Selective Transfer Hydrogenation of Alkynes

Xuge Zhang,‡[ab] He Lin,‡[c] Jian Zhang,‡*[b] Yajun Qiu,[a] Zedong Zhang,[a] Qi Xu,[a] Ge Meng,[b] Wensheng Yan,[d] Lin Gu,[e] Lirong Zheng,[f] Dingsheng Wang,*[a] Yadong Li[a]

[a] *Department of Chemistry, Tsinghua University, Beijing 100084, China.*
[b] *College of Chemistry and Materials Engineering, Wenzhou University, Wenzhou, Zhejiang 325035, China.*
[c] *State Key Laboratory of Chemistry and Utilization of Carbon Based Energy Resources; Key Laboratory of Advanced Functional Materials, Autonomous Region; Institute of Applied Chemistry, College of Chemistry, Xinjiang University, Urumqi, 830046, Xinjiang, China.*
[d] *National Synchrotron Radiation Laboratory, CAS Center for Excellence in Nanoscience, University of Science and Technology of China, Hefei 230029, China.*
[e] *Beijing National Laboratory for Condensed Matter Physics, Institute of Physics, Chinese Academy of Sciences, Beijing 100190, China.*
[f] *Beijing Synchrotron Radiation Facility, Institute of High Energy Physics, Chinese Academy of Sciences, Beijing 100049, China.*
‡ *These authors contributed equally to this work.*
* *Corresponding authors. E-mail: zhangjian@wzu.edu.cn;*
wangdingsheng@mail.tsinghua.edu.cn

Table of Contents

1. Experimental Section

1.1 Materials

Al_2O_3 (γ-phase, 20 nm, Aladdin), sodium hydroxide (NaOH, 99%, Sinopharm Chemical), copper(II) chloride dihydrate ($CuCl_2 \cdot 2H_2O$, 99%, Sinopharm Chemical), melamine (99%, Macklin Biochemical), formaldehyde solution (37 wt% in H_2O, stabilized with 10-15% methanol, J&K Chemical), ethanol (EtOH, ≥ 99.7%, Sinopharm Chemical), ammonia-borane (NH_3-BH_3, 97%, Energy Chemical), dodecane (99%, J&K Chemical) and alkyne reagents (analytic grade) were all obtained from commercial suppliers and used as received without further purification.

1.2 Synthesis of melamine-formaldehyde resin (MF) and pure CN

The preparation of MF followed a modified synthetic method in the literature[1]. In a general procedure, a mixed solution was obtained by dispersing melamine (3.0 g), formaldehyde solution (13 mL, 37 wt.% in H_2O, stabilized with 10-15% methanol) and NaOH aqueous solution (1.25 mL, 0.1 mol/L) in deionized water (14 mL) under ultrasonic vibration. The formed suspension was centrifuged after the mix solution heated at 65 ^oC for 1 h under stirring, and further washed with water and ethanol for one time respectively. The recovered solid was finally dried in a vacuum oven for 24 h to afford the MF.

1.3 Synthesis of [Cu]/MF and Cu$_1$/CN

To prepare [Cu]/MF, a mixed solution was obtained by dispersing 3.0 g melamine, 13 mL formaldehyde solution (37 wt.% in H_2O, stabilized with 10-15% methanol) and 1.25 mL NaOH aqueous solution (0.1 mol/L) in 14 mL water. After adequate ultrasonic vibration, the mixture was then heated at 65 ^oC for 20 min under vigorous stirring. Upon completion, $CuCl_2 \cdot 2H_2O$ (132.0 mg) was added into the mixture as soon as possible under continuous stirring. Raising the reaction temperature up to 105 ^oC and keeping evaporating 12 h to make sure the solvent removed. The remained solid was [Cu]/MF. The obtained [Cu]/MF was finally pyrolyzed in N_2 atmosphere at

400 °C for 2 h to afford the Cu$_1$/CN catalyst for further characterizations and catalysis tests.

1.4 Synthesis of [Cu]/MF/Al$_2$O$_3$ and Cu$_1$/CN/Al$_2$O$_3$

To prepare [Cu]/MF/Al$_2$O$_3$, Al$_2$O$_3$ powder (500.0 mg, γ-phase, 20 nm, Aladdin) was firstly dispersed in 14 mL deionized water under ultrasonic vibration to form the uniform suspension. Then, 3.0 g melamine, 13 mL formaldehyde solution (37 wt.% in H$_2$O, stabilized with 10-15% methanol) and 1.25 mL NaOH aqueous solution (0.1 mol/L) was added into the suspension. After adequate ultrasonic vibration, the mixture was heated at 65 °C for 30 min under vigorous stirring, during which the white color of the mixture changed to be lighter owing to the dissolution of melamine by reacting with formaldehyde. The mixture was next shifted to ambient temperature, and CuCl$_2$·2H$_2$O (52.6 mg) was added as soon as possible under vigorous stirring, which changed the mixture to deep green. After 10 min, the mixture was quickly centrifuged to keep the residual and further washed with deionized water and ethanol for one time respectively. The recovered light blue solid was then dried in a vacuum oven for at least 24 h to provide [Cu]/MF/Al$_2$O$_3$ for further characterizations. The obtained [Cu]/MF/Al$_2$O$_3$ was finally pyrolyzed under N$_2$ atmosphere in tube furnace at 400 °C (5 °C/min increased from ambient temperature) for 2 h to afford the final light grey Cu$_1$/CN/Al$_2$O$_3$ catalyst for further characterizations and catalysis tests.

1.5 Synthesis of Cu$_1$/Al$_2$O$_3$

To prepare Cu$_1$/Al$_2$O$_3$, Al$_2$O$_3$ powder (500.0 mg, γ-phase, 20 nm, Aladdin) was firstly dispersed in 15 mL deionized water under ultrasonic vibration to form the uniform suspension. Then, CuCl$_2$·2H$_2$O (52.6 mg) was dissolved in 5 mL deionized water, and the obtained solution was added dropwise into the Al$_2$O$_3$ suspension under vigorous stirring at ambient temperature. After contineously stirring for 12 h, the mixture was centrifuged to keep the residual and further washed with deionized water for one time. The recovered solid was then dried in a vacuum oven for at least 24 h and further treated under N$_2$ atmosphere in tube furnace at 400 °C (5 °C/min increased from

ambient temperature) for 2 h to afford the final Cu_1/Al_2O_3 catalyst for further characterizations and catalysis tests.

1.6 Measurements of transfer hydrogenation reactions

In a typical procedure, to a 10 mL glass bottle equipped with a stir bar, $Cu_1/CN/Al_2O_3$ (16.9 mg, Cu = 1.0 mol%) and alkynes (0.2 mmol, 22.0 μL) were mixed with EtOH (4.0 mL) under ultrasonic vibration to form a uniform suspension. Then NH_3-BH_3 (1.0 mmol, 30.9 mg) was added into the suspension, and kept the bottle sealed loosely. The mixture was heated at 70 °C for 8 h. After the reaction was completed, the reaction mixture was analyzed by GC and GC-MS with dodecane as the internal standard.

1.7 Recycling test of $Cu_1/CN/Al_2O_3$

Upon the completion of the reaction, the $Cu_1/CN/Al_2O_3$ catalyst was recovered by centrifuging from the reaction mixture, and washed with EtOH for three times. The recovered catalyst was redispersed in 4.0 mL EtOH with phenylacetylene (0.2 mmol) under ultrasonic vibration to form a uniform suspension which was transferred into a 10 mL glass bottle equipped with a stir bar. Next, NH_3-BH_3 (1.0 mmol, 30.1 mg) was added into the suspension, and the mixture was heated at 70 °C for 4 h. After that, the reaction mixture was analyzed by GC and GC-MS with dodecane as the internal standard. The same operation procedure was adopted for next four recycling runs.

1.8 Characterization Instruments

TEM images were taken from a Hitachi H-800 transmission electron microscope operated at 100 kV. HR-TEM, STEM and EDX elemental mapping characterizations were carried out on a JEOL JEM-2100F field emission transmission electron microscope operated at 200kV. The AC-HAADF STEM characterization was conducted on a Titan 80-300 scanning/transmission electron microscope operated at 300 kV, equipped with a probe spherical aberration corrector. XRD data were acquired from a Rigaku RU-200b X-ray powder diffractometer with Cu Kα radiation

(λ = 1.5406 Å). ICP-OES measurements were conducted on a Thermo Fisher iCAP™ 7000 Series ICP-OES analyzer. EXAFS and XANES spectra at Cu K-edge were collected at the 1W1B station in Beijing Synchrotron Radiation Facility (BSRF) in fluorescence excitation mode (Cu_1/CN, Cu_1/Al_2O_3 and $Cu_1/CN/Al_2O_3$) and transmission mode (Cu foil, CuO and Cu_2O) using a fixed-exit Si (111) double crystal monochromator. The incident X-ray beam was monitored by an ionization chamber filled with N_2, and the acquired EXAFS data were processed according to the standard procedures using the ATHENA module implemented in the IFEFFIT software packages. XPS data were collected from a Thermo Fisher Scientific ESCALAB 250Xi XPS System, and the binding energy of the C 1s peak at 284.8 eV was taken as an internal reference. FT-IR spectroscopy was performed on a Bruker V70 infrared spectrometer in the frequency of 600-4000 cm^{-1}. The GC analysis was conducted on a Thermo Trace 1300 series GC with a FID detector using a capillary column (TG-5MS, from Thermo Scientific, length 30 m, i.d. 0.25 mm, film 0.25 μm). The GC-MS analysis was carried out on a ISQ GC-MS with a ECD detector (Thermo Trace GC Ultra) using a capillary column (TG-5MS, from Thermo Scientific, length 30 m, i.d. 0.25 mm, film 0.25 μm).

2. Computational Details

These first-principles calculations in this study were based on density functional theory (DFT) using the Perdew-Burke-Ernzerholf (PBE) functional[2] as implemented in the Vienna Ab Initio Simulation Package (VASP)[3] . We used a plane-wave basis set with the projector augmented plane-wave (PAW) method. The plane-wave cutoff energy was set to 400 eV, and the convergence criteria for the electronic self-consistent iterations and forces were 1×10^{-5} eV and 0.01 eV/ Å, respectively. The SA Cu coordination structures were simulated using $6 \times 6 \times 1$ supercell with a vacuum space of 20 Å, and the Brillouin zone was sampled using a $3 \times 3 \times 1$ Γ-centered k-point mesh. The energy barrier was determined using the Climbing-Image Nudged Elastic Band (CINEB) method[4, 5].

3. Supplementary Figures and Tables
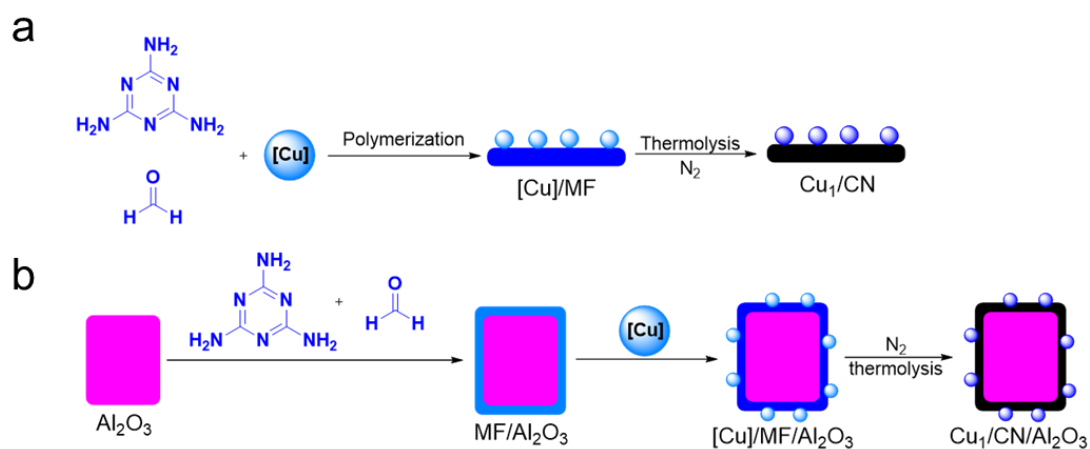
Figure S1. Synthetic strategy of Cu_1/CN (a) and $Cu_1/CN/Al_2O_3$ (b).

We utilize Al_2O_3 matrix as the template for in-situ polymerization reaction of melamine and formaldehyde to synthesize the $Cu_1/CN/Al_2O_3$ catalyst. A MF layer can successfully coat on the surface of Al_2O_3 matrix to make the formed CN carrier be thinner with less amount of doped N atoms[6].
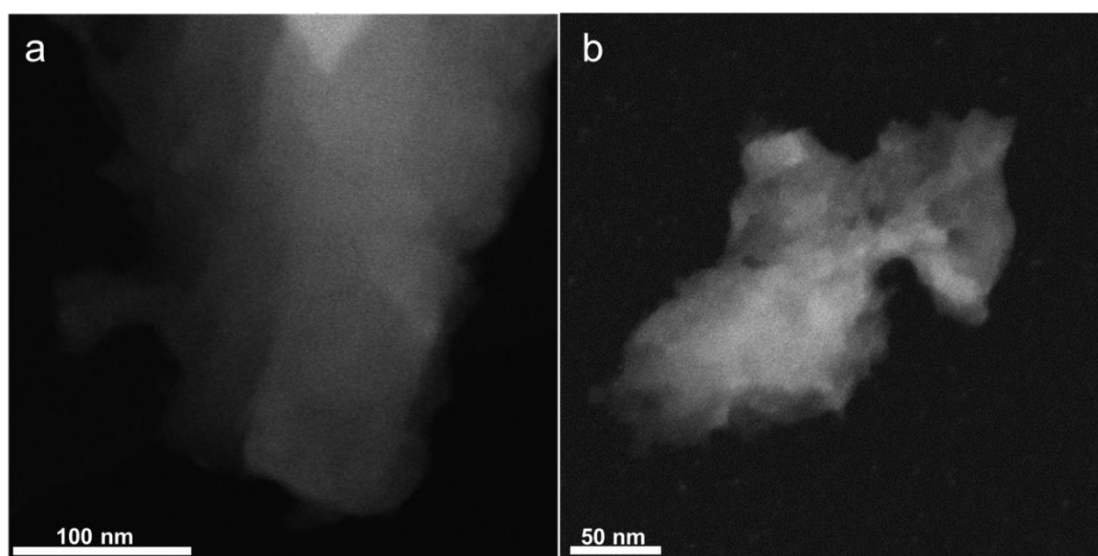
**Figure S2.** STEM images of Cu_1/CN in different magnifications.

It can be clear observed that the Cu_1/CN presents the irregular nanoblock morphology, and no copper or copper oxide nanoparticles can be found on it.
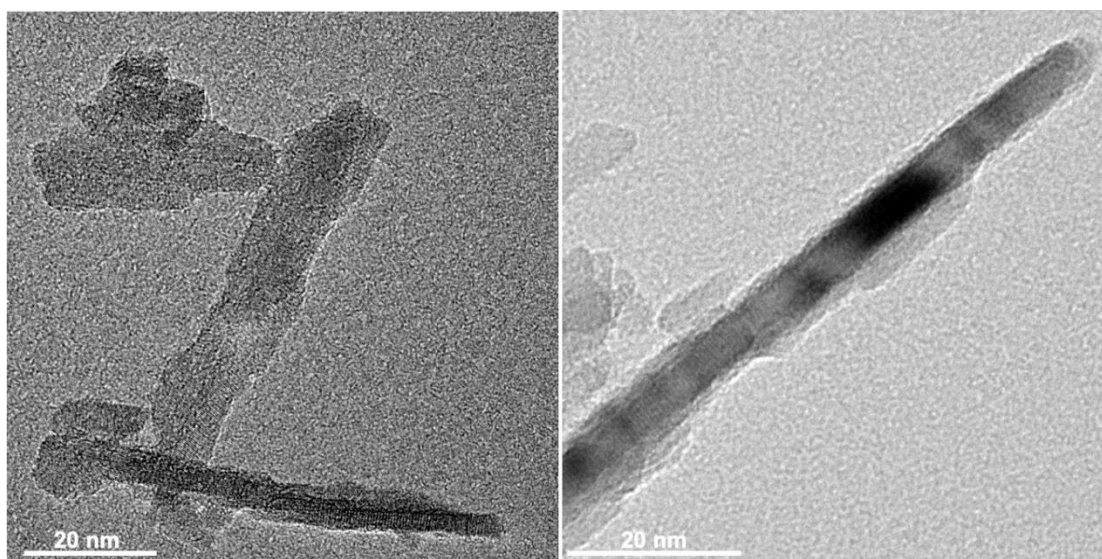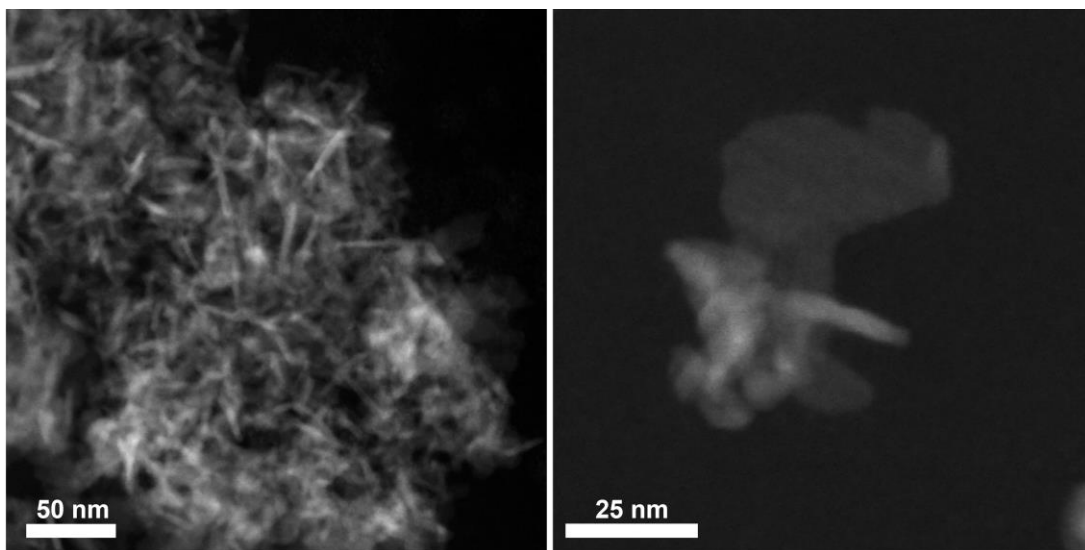
Figure S3. HR-TEM images of [Cu]/MF/Al$_2$O$_3$ in different magnifications.

Obviously, a thin MF coating layer can be distinguished from the Al$_2$O$_3$ matrix after the in-situ polymerization of melamine and formaldhyde.
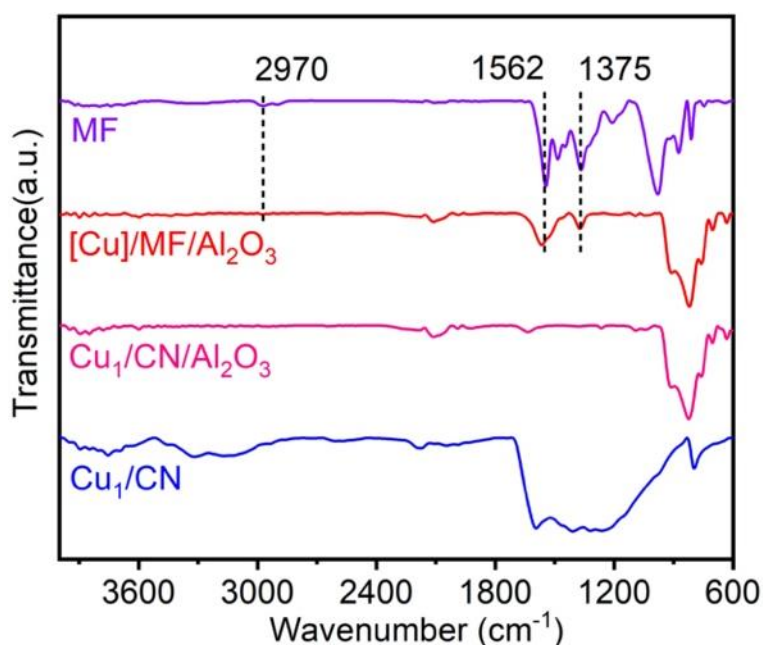
**Figure S4.** FT-IR measurements of SAS Cu catalysts before and after pyrolysis.

As can be seen from FT-IR spectra, three adsorption bands at ~297, ~1563 and 1375 cm^{-1} simultaneously appear on MF and [Cu]/MF/Al$_2$O$_3$. These bands can be assigned to stretching vibration peaks of C-H, triazine ring and C-N moieties in MF[7]. Therefore, the composition of coating layers on the Al$_2$O$_3$ is determined to be MF. When [Cu]/MF/Al$_2$O$_3$ samples are pyrolyzed in N$_2$ at 400 ^{o}C for 2 h, these three bands disappeared in the FI-IR spectra of obtained Cu$_1$/CN/Al$_2$O$_3$ catalyst, which is similar to Cu$_1$/CN, suggesting the transformation of MF layers into CN materials.

Figure S5. STEM images of $Cu_1/CN/Al_2O_3$ in different magnifications.

It shows that no observable copper or copper oxide nanoparticles can be found on the $Cu_1/CN/Al_2O_3$ catalyst.
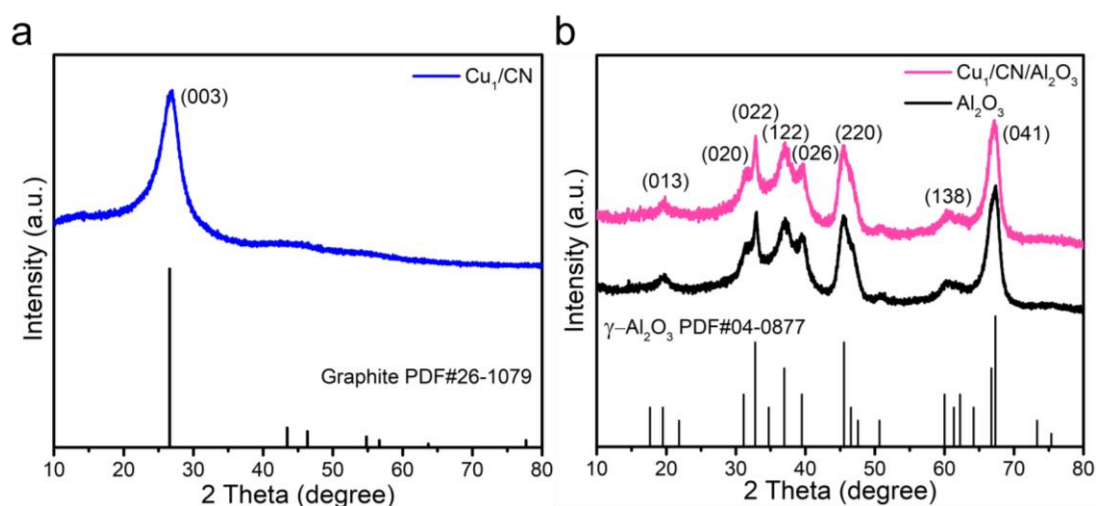
Figure S6. XRD studies of synthesized SAS Cu catalysts. (a) The XRD pattern of Cu_1/CN. (b) XRD patterns of $Cu_1/CN/Al_2O_3$ in comparison with pure Al_2O_3.

There are no Cu characteristic signals appearing in XRD patterns of Cu_1/CN and $Cu_1/CN/Al_2O_3$ catalysts. The notable peak at around 27 degree in the XRD pattern of Cu_1/CN can be assigned to the feature of graphitic CN materials[8]. $Cu_1/CN/Al_2O_3$ and pure Al_2O_3 host exhibit identical XRD patterns which belong to γ-Al_2O_3 phase (PDF#04-0877), indicating the stability of used Al_2O_3 host during the preparation of the $Cu_1/CN/Al_2O_3$ catalyst.
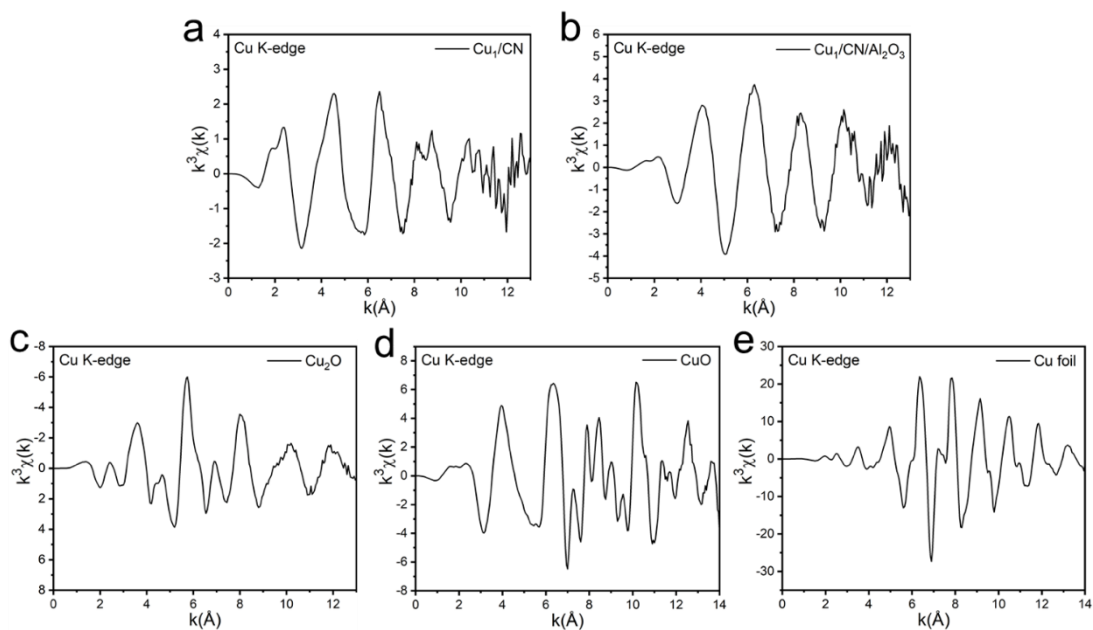
Figure S7. The k^3-weighted EXAFS in k-space at the Cu K-edge for the Cu_1/CN (a), Cu_1/CN/Al_2O_3 (b), Cu_2O (c), CuO (d) and Cu foil (e).

Table S1. Fitting parameters of the N 1s XPS spectra in Fig. 2e.

| Sample	Peak type	Position (eV)	FWHM	Area	Proportion (%)
Cu_1/CN	pyridinic-N	398.6	1.6	1.62	65
	pyrrolic-N	399.8	1.6	0.55	22
	graphitic-N	400.9	1.6	0.32	13
Cu_1/CN/Al_2O_3	pyridinic-N	398.7	2.0	1.30	61
	pyrrolic-N	399.8	2.0	0.54	25
	graphitic-N	400.8	2.0	0.31	14
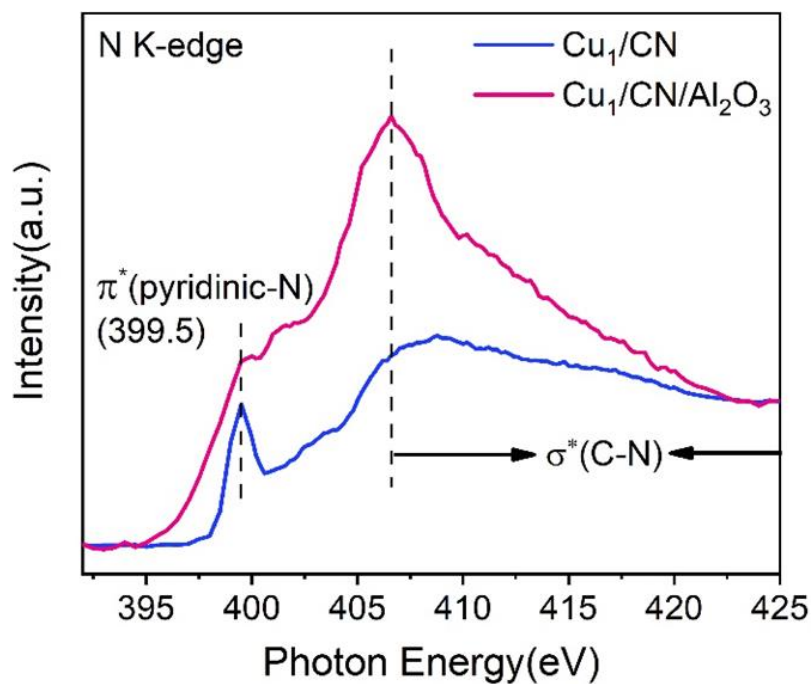
Figure S8. N K-edge sXAS spectra of Cu_1/CN and $Cu_1/CN/Al_2O_3$ catalysts.

As we can see from the sXAS spectra, $Cu_1/CN/Al_2O_3$ gains much less intensity of π^*-transition (pyridinic-N) than Cu_1/CN catalyst which means the lower content of N atoms.

Table S2. Elemental analysis results of synthesized SA Cu catalysts.

Catalyst	N content (wt%)	C content (wt%)	N/Cu[a]
Cu_1/CN	30.77	30.25	18.66
$Cu_1/CN/Al_2O_3$	1.04	2.07	1.07

[a]Mass ratio.
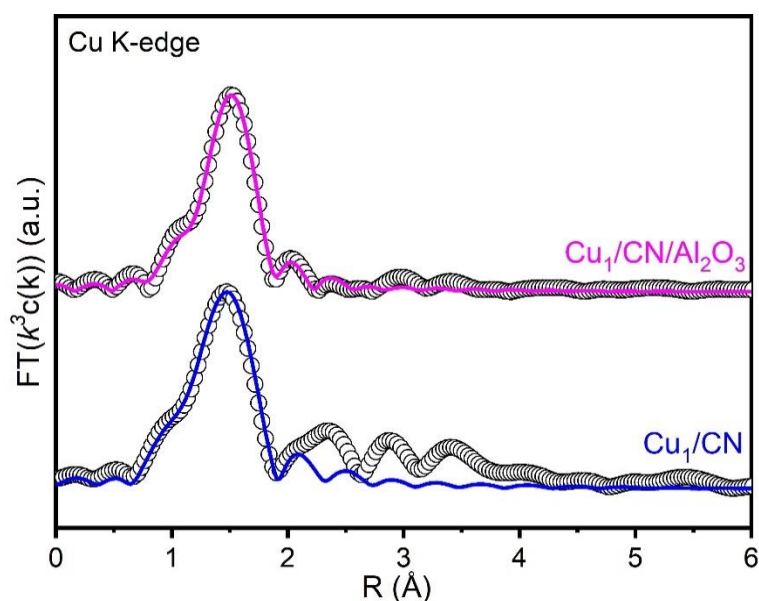
Sample	Path	CN	R (Å)	σ^2 (10^{-3}Å^2)	ΔE_0 (eV)	R factor
Cu$_1$/CN/Al$_2$O$_3$	Cu-N	1.9	2.00	5.3	-1.0	0.007
Cu$_1$/CN	Cu-N	3.2	1.94	5.1	-1.5	0.005

Figure S9. Cu K-edge EXAFS fitting analysis of Cu$_1$/CN and Cu$_1$/CN/Al$_2$O$_3$. S$_0^2$ is the amplitude reduction factor; CN is the coordination number; R is interatomic distance (the bond length between central atoms and surrounding coordination atoms); σ^2 is Debye-Waller factor (a measure of thermal and static disorder in absorber-scatterer distances); ΔE_0 is edge-energy shift (the difference between the zero kinetic energy value of the sample and that of the theoretical model). R factor is used to value the goodness of the fitting. Error bounds that characterize the structural parameters obtained by EXAFS spectroscopy were estimated as CN $\pm$ 20%; R $\pm$ 1%; σ^2 $\pm$ 20%; ΔE_0 $\pm$ 20%.

According to the fitting results, it can be determined that SA Cu species in Cu$_1$/CN exist as the Cu-N$_3$ and Cu-N$_4$ coordination structure with Cu-N bond distance as ~1.94 Å and SA Cu species in Cu$_1$/CN/Al$_2$O$_3$ exist as the Cu-N$_2$ coordination structure with Cu-N bond distance as ~2.00 Å.
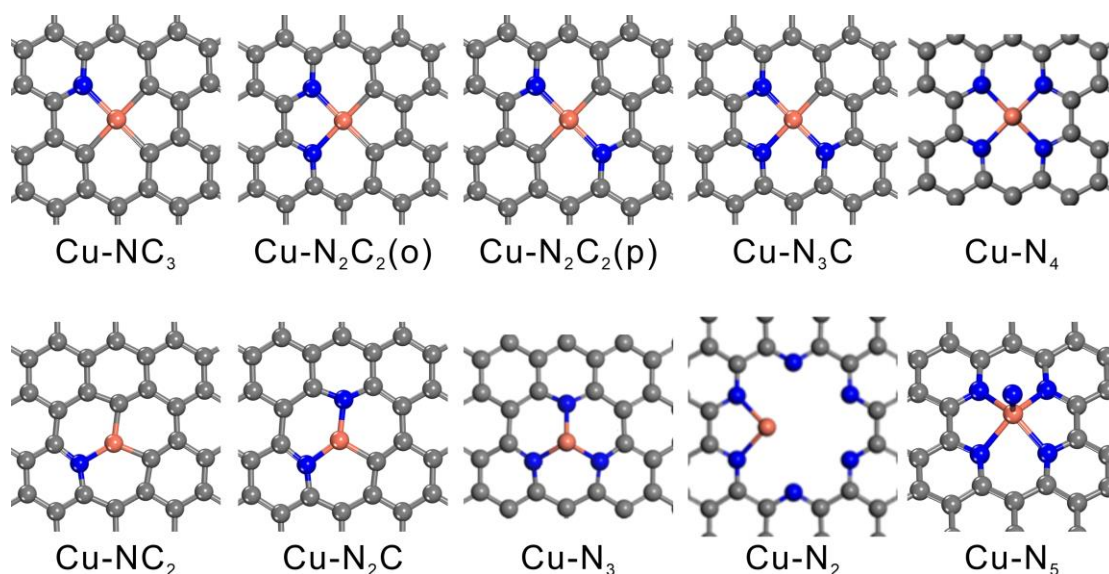
Figure S10. Simulation of SA Cu centers on CN with different coordination structures.

Table S3. DFT calculation analyses on the charge of SA Cu centers in different coordination structures.

Models	$Cu-NC_3$	$Cu-N_2C_2(o)$	$Cu-N_2C_2(p)$	$Cu-N_3C$	$Cu-N_4$
Charge of Cu (e)	0.730	0.792	0.841	0.900	0.955
Models	$Cu-NC_2$	$Cu-N_2C$	$Cu-N_3$	$Cu-N_2$	$Cu-N_5$
Charge of Cu (e)	0.592	0.645	0.668	0.712	0.990

It is indicated that the $Cu-N_5$ structure displays the higher charge of Cu than the $Cu-N_4$ structure, whereas $Cu-N_2C$ and $Cu-NC_2$ structures display the lower charge of Cu than the $Cu-N_3$ structure. These structures cannot be the coordination structurs of SA Cu centers in $Cu_1/CN/Al_2O_3$ because they are inconsistent with the observation from Cu $2p_{3/2}$ XPS spectra that the oxidation state of Cu in $Cu_1/CN/Al_2O_3$ is medium between that of two Cu species in Cu_1/CN (major $Cu-N_3$ structure with a few $Cu-N_4$ structure as repored in previous studies). As for $Cu-N_3C$, $Cu-N_2C_2$ and $Cu-NC_3$ structures, although their charge of Cu are right between that of $Cu-N_3$ and $Cu-N_4$ structures, they are all saturated coordination. Such saturated coordination cannot provide suitable adsorption sites for hydrogen species and alkyne substrates to realize the transfer hydrogenation reaction as proved in Fig. 5. Therefore, they cannot either be the coordination structure of SA Cu centers in $Cu_1/CN/Al_2O_3$. On the basis of above results, we believe that SA Cu centers in $Cu_1/CN/Al_2O_3$ predominantly exist as the $Cu-N_2$ structure with more unsaturated coordination sites for achieving the transfer hydrogenation of alkynes.
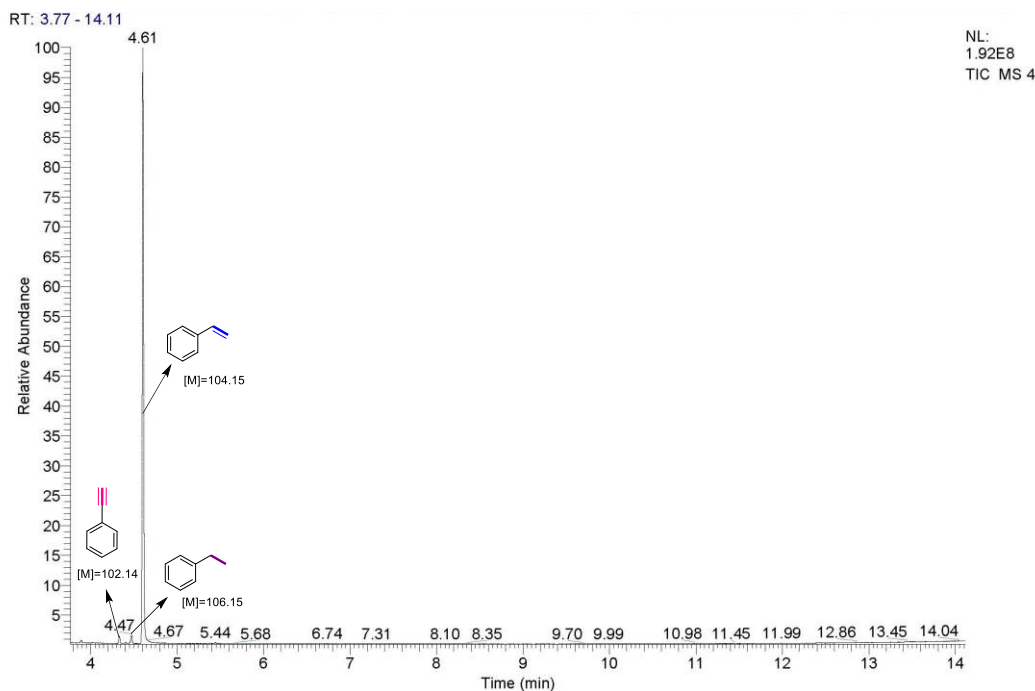
Figure S11. GC-MS analysis on the transfer hydrogenation reaction upon completion. Reaction conditions: phenylacetylene (0.2 mmol), AB (1.0 mmol), $Cu_1/CN/Al_2O_3$ (16.9 mg, Cu = 1.0 mol%) in ethanol (4.0 mL) at 70 °C for 8.0 h.

Apparently, the main product styrene can be detected in the reaction mixture, demonstrating the good selectivity of the $Cu_1/CN/Al_2O_3$ catalyst.

Table S4. Performance comparison of heterogeneous catalysts for transfer semihydrogenation of alkynes using ammonia borane as the hydrogen source.

Catalyst	Active metal	T (°C)	*time*	Conv. (%)	Sel. (%)	TON	Ref.
Pd-SAs/CNF	Pd	50	3 h	99	99	1962	9
Au/TiO$_2$	Au	25	0.5 h	100	>94	94	10
TiO$_2$/Pt/TiO$_2$	Pt	30	4 h	98	96	108	11
CeO$_2$ nanotube/Pd@MIL-52(Al)	Pd	25	1 min	100	96	16	12
[a]CuPd@ZIF-8	Pd	25	3 min	99	96	20397	13
Pd/UiO-66(Hf)	Pd	25	30 min	>99	99	91	14
[b]Cu NPs	Cu	40	3 h	99	97	10	15
[b]Cu/CuO	Cu	50	45 min	100	99	2	16
Cu$_1$/CN/Al$_2$O$_3$	**Cu**	**70**	**8 h**	**99**	**98**	**74**	**This work**

[a]Light > 400 nm, 160 mW/cm^2. [b]The recyclability is poor.

As it can be seen that most heterogeneous catalysts reported for transfer semihydrogenation of alkynes with ammonia borane are based on noble metals like

Pd, Au and Pt. Only two non-noble metal (Cu) based catalysts have been applied successfully in such reaction, but suffer from the poor catalytic efficiency (low TON values) and recyclability.
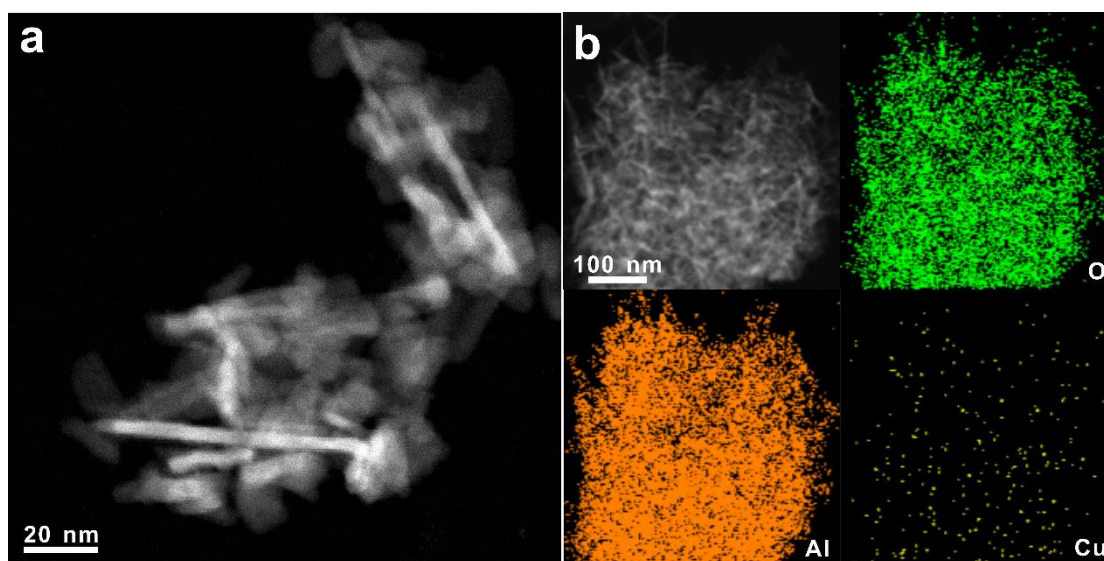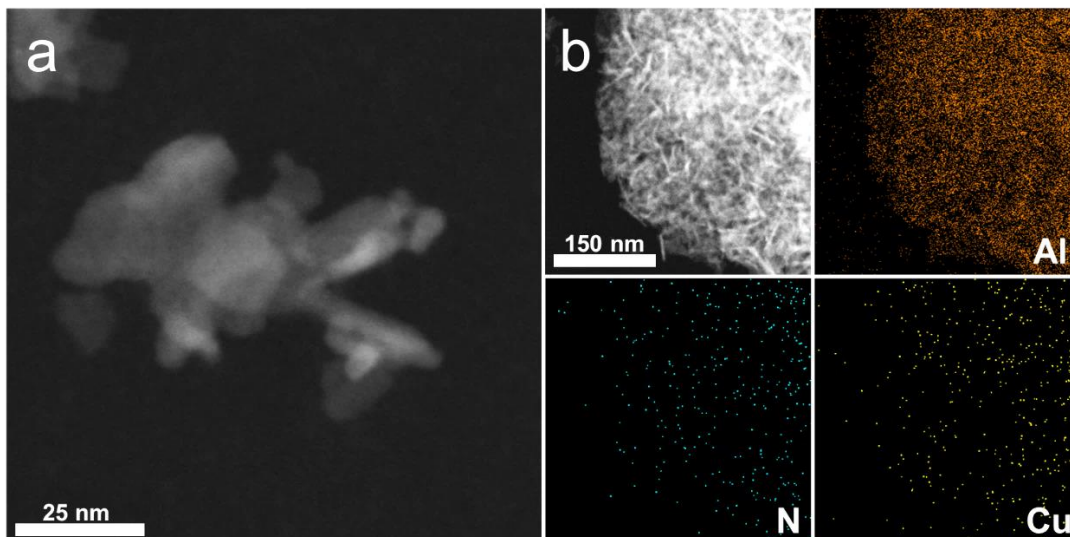

Figure S12. Characterizations of Cu_1/Al_2O_3. (a) STEM image of Cu_1/Al_2O_3. (b) EDX elemental mapping analysis of Cu_1/Al_2O_3.

As it can be seen, the Cu species disperse homogeneously on Al_2O_3 support in the Cu_1/Al_2O_3 catalyst.
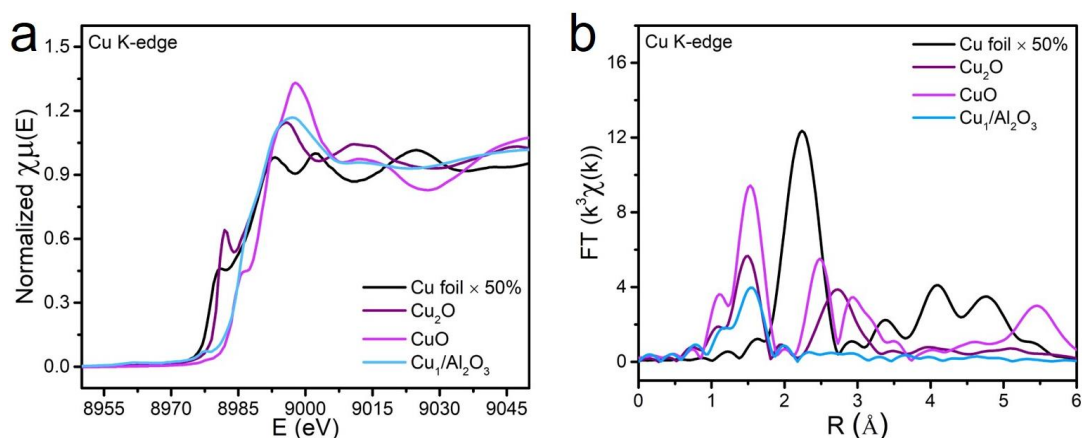
Figure S13. XAS measurements of Cu_1/Al_2O_3. (a) XANES spectra of Cu_1/Al_2O_3 with CuO, Cu_2O and Cu foil as references at Cu K-edge. (b) FT-EXAFS spectra of Cu_1/Al_2O_3 with CuO, Cu_2O and Cu foil as references at Cu K-edge.

As it can be seen, there is only one primary peak attributed to the Cu-O bond (~1.5 Å) but no other peaks of the Cu-Cu bond (~2.1 Å) being observed for Cu_1/Al_2O_3, proving the presence of SA Cu species.

Figure S14. Characterizations of recovered $Cu_1/CN/Al_2O_3$. (a) STEM image of recovered $Cu_1/CN/Al_2O_3$. (b) EDX elemental mapping analysis of recovered $Cu_1/CN/Al_2O_3$.

It can be concluded that SA Cu species remain in the recovered catalyst without aggregation, indicating the good stability of the $Cu_1/CN/ Al_2O_3$ catalyst.
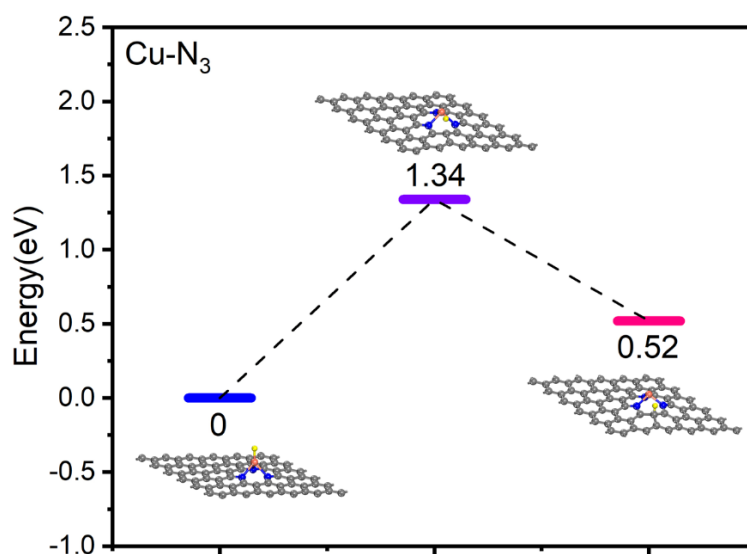
Figure S15. DFT calculation studies on the spillover hydrogenation pathway over Cu_1/CN as the first step of transfer hydrogenation of phenylacetylene.

The hydrogen specie shifts from the Cu center to the ortho carbon to give the adsorption site for the phenylacetylene molecular over Cu_1/CN catalyst.

4. References

1. S. Mou, Y. Lu and Y. Jiang, *Appl. Surf. Sci.*, 2016, **384**, 258-262.
2. J. P. Perdew, K. Burke and M. Ernzerhof, *Phys. Rev. Lett.*, 1996, **77**, 3865-3868.
3. G. Kresse and J. Furthmüller, *Phys. Rev. B: Condens. Matter Mater. Phys.*, 1996, **54**, 11169-11186.
4. G. Henkelman, B. P. Uberuaga and H. Jónsson, *J. Chem. Phys.*, 2000, **113**, 9901-9904.
5. G. Henkelman and H. Jónsson, *J. Chem. Phys.*, 2000, **113**, 9978-9985.
6. J. Zhang, C. Zheng, M. Zhang, Y. Qiu, Q. Xu, W.-C. Cheong, W. Chen, L. Zheng, L. Gu, Z. Hu, D. Wang and Y. Li, *Nano Res.*, 2020, **13**, 3082-3087.
7. T. Zhang, D. Zhang, X. Han, T. Dong, X. Guo, C. Song, R. Si, W. Liu, Y. Liu and Z. Zhao, *J. Am. Chem. Soc.*, 2018, **140**, 16936-16940.
8. Z. Shen, H. Zhao, Y. Liu, Z. Kan, P. Xing, J. Zhong and B. Jiang, *React. Chem. Eng.*, 2018, **3**, 34-40.
9. Z. Zhang, M. Zhou, Y. Chen, S. Liu, H. Wang, J. Zhang, S. Ji, D. Wang and Y. Li, *Sci. China Mater.*, 2021, **64**, 1919-1929.
10. E. Vasilikogiannaki, I. Titilas, G. Vassilikogiannakis and M. Stratakis, *Chem. Commun.*, 2015, **51**, 2384-2387.
11. H. Liang, B. Zhang, H. Ge, X. Gu, S. Zhang and Y. Qin, *ACS Catal.*, 2017, **7**, 6567-6572.
12. X. Li, L. Song, D. Gao, B. Kang, H. Zhao, C. Li, X. Hu and G. Chen, *Chemistry*, 2020, **26**, 4419-4424.
13. L. Li, W. Yang, Q. Yang, Q. Guan, J. Lu, S.-H. Yu and H.-L. Jiang, *ACS Catal.*, 2020, **10**, 7753-7762.
14. V. R. Bakuru, D. Samanta, T. K. Maji and S. B. Kalidindi, *Dalton Trans.* , 2020, **49**, 5024-5028.
15. B. Y. Park, T. Lim and M. S. Han, *Chem. Commun.*, 2021, **57**, 6891-6894.
16. S. Rej, M. Madasu, C. S. Tan, C. F. Hsia and M. H. Huang, *Chem Sci*, 2018, **9**, 2517-2524.